[5] Matthiesson, L., "Akustische Versuche, die kleinsten Traversalwellen der Flussigkeiten betreffend," *Annalen der Physik und Chemie*, Vol. 134, 1868, pp. 107–117.

[6] Matthiesson, L., "Uber die Transverslchwingungen tonender tropfbarer und elasticher Flussigkeiten," *Annalen der Physik und Chemie*, Vol. 141, 1870, pp. 375–393.

[7] Benjamin, T. B. and Ursell, F., "The Stability of a Plane Free Surface of a Liquid in Vertical Periodic Motion," *Proceedings of the Royal Society*, Vol. A225, 1954, pp. 505–517.

[8] Penney, W. G. and Price, A. T., "Finite Periodic Stationary Gravity Waves in a Perfect Liquid," *Philosophical Transactions of the Royal Society*, Vol. 244, 1952, pp. 254–284.

[9] Skalak, R. and Yarymovych, M., "Forced Large Amplitude Surface Waves," *Fourth U.S. National Congress on Applied Mechanics*, June 1962, pp. 1411–1418.

[10] Dodge, F. T., Kana, D. D., and Abramson, H. N., "Liquid Surface Oscillations in Longitudinally Excited Rigid Cylindrical Containers," *AIAA Journal*, Vol. 3, No. 4, April 1965, pp. 685–695.

[11] Bauer, H. F. and Woodward, J., "Fluid Behavior in a Longitudinally-excited Cylindrical Tank of Arbitrary Sector-Annular Cross Section," *AIAA Journal*, Vol. 8, No. 4, 1970, pp. 713–719.

[12] Bhuta, P. G. and Koval, L. R., "Coupled Oscillations of a Liquid with a Free Surface in a Tank Having a Flexible Bottom," *Zeitschrift fuer Angewandte Mathematik, und Physik*, Vol. 15, 1964, pp. 466–480.

[13] Bhuta, P. G. and Koval, L. R., "Hydroelastic Solution of the Sloshing of a Liquid in a Cylindrical Tank," *Journal of the Acoustical Society America*, Vol. 36, No. 11, 1964, pp. 2071–2079.

[14] Siekmann, J. and Chang, S. C., "On Liquid Sloshing in a Cylindrical Tank with a Flexible Bottom Under Strong Capillary and Weak Gravity Conditions," *Journal of the Astronautical Sciences*, Vol. 14, No. 4, 1967, pp. 167–172.

[15] Bauer, H. F., Hsu, T. M., and Wang, J. T. S., "Liquid Sloshing in Elastic Containers," CR-882, 1967, NASA.

[16] Bauer, H. F., Siekmann, J., and Wang, J. T. S., "Axisymmetric Hydroelastic Sloshing in an Annular Cylindrical Container," *Journal of Spacecraft and Rockets*, Vol. 5, No. 8, Aug. 1968, pp. 981–983.

[17] Tong, P. and Fung, Y. C., "The Effect of Wall Elasticity and Surface Tension on the Forced Oscillations of a Liquid in a Cylindrical Container," SM-64-40, Oct. 1964, Graduate Aerospace Labs., California Inst. of Technology, Pasadena, Calif.

[18] Bauer, H. F., "Nonlinear Propellant Sloshing in a Rectangular Container of Infinite Length," *Developments in Theoretical and Applied Mechanics, Proceedings of the Third Southeastern Conference*, Vol. 3, 1966.

[19] Fung, Y. C., *Foundations of Solid Mechanics*, Prentice-Hall, Englewood Cliffs, N.J., 1965, pp. 456–463.

[20] Timoshenko, S. and Woinowsky-Krieger, S., *Theory of Plates and Shells*, McGraw-Hill, New York, 1959, pp. 1–3.

[21] Chang, S.-S., "Longitudinally Excited Nonlinear Liquid Motion in a Circular Cylindrical Tank with Elastic Bottom," Ph.D. thesis, Dec. 1969, Georgia Inst. of Technology, Atlanta, Ga.

[22] Bolotin, V. V., *Dynamic Stability of Elastic Systems*, Holden-Day, San Francisco, Calif., 1964.

[23] Dodge, T. F., Kana, D. D., and Abramson, H. N., "Liquid Surface Oscillations in Longitudinally Excited Rigid Cylindrical Containers," TR 2, Contract NAS8-11045, SWRI Project 13-02-1391, 1964, Southwest Research Inst.

DECEMBER 1971 AIAA JOURNAL VOL. 9, NO. 12

Free Vibrations of Pressure Loaded Paraboloidal Shells

DAVID S. MARGOLIAS* AND VICTOR I. WEINGARTEN†
University of Southern California, Los Angeles, Calif.

The finite element method is used to analyze the free vibrations of thin, isotropic, paraboloidal shells of revolution subjected to a uniform external pressure loading. The continuous shell is mathematically subdivided into discrete circular frusta whose meridional shape exactly duplicates that of the undeformed paraboloid. Sanders' shell (strain-displacement) equations are used, and both the initial loading (stress) and perturbation displacement (eigenvalue) problems are linearized and are solved on the digital computer. Numerical solutions are compared to experimental data gathered from vibration tests conducted on a variety of paraboloidal shells loaded by a uniform external pressure. In view of the imperfect clamped boundary condition achieved during the tests, the agreement between the two results is very good. The shape of the natural frequency-harmonic curve in every case was found to conform to that theoretically predicted for shells having a positive Gaussian curvature for their meridians. Increasing the external pressure was found to lower the natural frequencies of the shell, in a nearly linear relation at low-pressures, but nonlinearly as the pressure approached the critical buckling value.

Nomenclature

a_i = coefficients in assumed displacement functions
E = elastic modulus
h = shell thickness
l = meridional length of the finite element
$M_{\theta\theta}{}^e, M_{ss}{}^e$ = initial load state circumferential and meridional moment resultants
m = mode of vibration
$N_{\theta\theta}{}^e, N_{ss}{}^e$ = initial load state circumferential and meridional stress resultants
n = harmonic (circumferential wave) number
p = uniform pressure loading
q_i = generalized displacements
r = shell middle surface radius
s = meridional coordinate
T = kinetic energy
t = time
U = strain energy
u,v,w = shell middle surface meridional, circumferential and normal displacements

Presented as Paper 71-214 at the AIAA 9th Aerospace Sciences Meeting, New York, January 25–27, 1971; submitted February 19, 1971; revision received August 2, 1971. The authors wish to express their appreciation to D. Sherman for his help in performing the experimental portion of this study. The writers also acknowledge the National Science Foundation for the grant which supported this investigation.

Index categories: Structural Stability Analysis; Structural Dynamic Analysis.

* Assistant Professor, Department of Civil Engineering.
† Associate Professor, Department of Civil Engineering.

v_s, v_θ, v_z = shell middle surface meridional, circumferential and normal velocities
W = work of the uniform pressure loading
β_s, β_θ = meridional and circumferential middle surface rotations
$\epsilon_{\theta\theta}, \epsilon_{ss}, \epsilon_{\theta s}$ = shell middle surface strains
φ = angle defining normal to shell middle surface
$\kappa_{\theta\theta}, \kappa_{ss}, \kappa_{\theta s}$ = shell middle surface curvatures and twist
ν = Poisson's ratio
θ = circumferential coordinate
ρ = mass density
ω = natural frequency

Matrices

$\{a\}$ = vector of coefficients in the assumed displacement functions
$\{Q\}$ = vector of generalized forces
$\{q\}$ = vector of generalized displacements
$[I]$ = identity matrix
$[K]$ = kinematic stiffness matrix
$[K_g]$ = geometric stiffness matrix
$[M]$ = inertia matrix
$[N]$ = uniform pressure work matrix
$[\psi]$ = matrix relating element nodal displacements to the coefficients in the assumed element displacement functions

Subscripts

e = refers to the initial load (equilibrium) state
p = refers to the final displacement (initial load + perturbed displacement) state

Introduction

BECAUSE of the complexity of the shell equilibrium equations, the solution of shell problems is not easily accomplished, and exact, closed form solutions exist only for select problems involving only the simplest of geometries, i.e., for cylindrical, conical and spherical shells. The solution of the more complex problems must be accomplished numerically, with extensive use frequently being made of the high-speed, large memory digital computer to perform the large amount of resulting computations.

The vibration analysis of a shell under the influence of an external loading is, of course, quite important since most structural applications involve combined load and dynamic environments. The importance of such analyses will further be shown in the results of this paper, wherein it will be seen that the external loading can have a marked effect on the dynamic characteristics of the shell. This effect has also been shown previously, although as might be expected from the preceding discussion, this has been done only for the simpler geometric shapes. Armenákas[1] and Armenákas and Herrmann[2] have performed such analyses for cylindrical shells, and Archer,[3] Archer and Famili,[4] and Okubo and Whittier[5] did the same for spherical shells.

The investigation reported on in this paper treats the problem of the vibrations of a paraboloidal shell of revolution subjected to an externally applied uniform pressure loading. Because of the more complex geometry of the paraboloid, the problem could only be solved using a numerical analysis. The finite element method, wherein the total energy of the shell is approximated as the sum of that of the elements into which the continuous structure has been mathematically subdivided, is used in the present analysis.

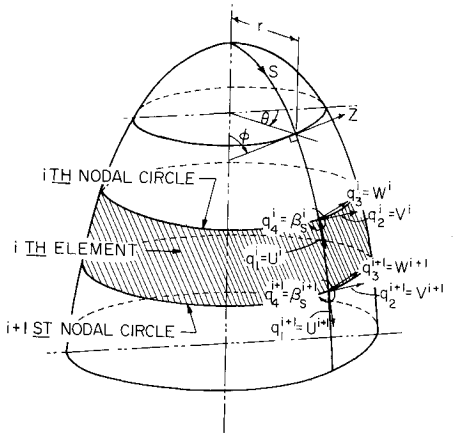

Fig. 1 Finite element model, shell coordinates and assumed nodal displacements.

Problem Statement

The paraboloidal shell is mathematically subdivided into circular frusta whose meridional shape exactly duplicates that of the paraboloid in the undeformed state. This hypothetical subdivision of the shell is accomplished by passing a series of planes through the shell surface and normal to the generating axis (axis of revolution). The resulting element, shown in Fig. 1, is bounded on each end by a nodal circle or node, the displacements of which are used to represent the modal displacements of the composite shell.

The vibration problem for an initially loaded shell is solved by analyzing two distinct but interdependent problems. The first of these is the solution of the initial (static) loading problem, i.e., determining the stresses and nodal displacements caused by the initial pressure loading. The second problem to be solved is the vibration (eigenvalue) problem, which is set up by perturbing the stressed shell from its initial displaced (equilibrium) state with small, harmonic oscillations superposed on the initial displacements. The buckling problem is solved as the limiting case of this problem, wherein the perturbation displacements are imposed at a zero natural frequency, i.e., the perturbation displacements are independent of time.

To reach the initial deformed state under the action of the uniform pressure loading, each node is assumed to have 3 degrees-of-freedom (displacements in the meridional and shell normal directions and the rotation of the meridian), with all asymmetric displacement components vanishing. For the general perturbation problem, the asymmetric (circumferential) displacement component is considered so that 4 degrees-of-freedom are taken at each node. However, because both the external loading and the shell are symmetric about the generating axis, it is possible to completely describe the circumferential coordinate dependence in terms of a complete Fourier series. With the formulation linearized, it is further possible to consider each of the terms of this series separately. Expressing the meridional dependence in terms of polynomial functions, the displacements assumed for the solution are

$$q_1 = u = (a_5 + a_6 s)e^{i\omega t}\cos n\theta \tag{1a}$$

$$q_2 = v = (a_7 + a_8 s)e^{i\omega t}\sin n\theta \tag{1b}$$

$$q_3 = w = (a_1 + a_2 s + a_3 s^2 + a_4 s^3)e^{i\omega t}\cos n\theta \tag{1c}$$

$$q_4 = \beta_s = [(a_2 - a_5 d\varphi/ds) + (2a_3 - a_6 d\varphi/ds)s + 3a_4 s^2]e^{i\omega t}\cos n\theta \tag{1d}$$

The third-order polynomial is used in the normal displacement function to satisfy rotation as well as displacement compatibility between adjacent elements. For the static ($\omega = 0$), symmetric ($n = 0$) initial load state these displacement functions reduce to

$$q_1{}^e = u^e = (a_5{}^e + a_6{}^e s); \quad q_2{}^e = v^e = 0 \tag{2a}$$

$$q_3{}^e = w^e = (a_1{}^e + a_2{}^e s + a_3{}^e s^2 + a_4{}^e s^3) \tag{2b}$$

$$q_4{}^e = \beta_s{}^e = [(a_2{}^e - a_5{}^e d\varphi/ds) + (2a_3{}^e - a_6{}^e d\varphi/ds)s + 3a_4{}^e s^2] \tag{2c}$$

Initial Load State

The shell (strain-displacement) equations used in this study were derived by Sanders[6] and are nonlinear in the displacements. For the linear analysis of the symmetric initial load state, Sanders' equations reduce to

$$\epsilon_{\theta\theta}{}^e = (1/r)[u^e \cos\varphi + w^e \sin\varphi] \tag{3a}$$

$$\epsilon_{ss}{}^e = [\partial u^e/\partial s + w^e d\varphi/ds] \tag{3b}$$

$$\epsilon_{\theta s}{}^e \equiv 0;\ \kappa_{\theta\theta}{}^e = -\beta_s{}^e \cos\varphi/r;\ \kappa_{ss}{}^e = -\partial\beta_s{}^e/\partial s;\ \kappa_{\theta s}{}^e \equiv 0 \tag{3c}$$

where the initial load state rotation is given by

$$\beta_s{}^e = [\partial w^e/\partial s - u^e d\varphi/ds] \tag{4}$$

With the middle surface shearing strain and twist so vanishing, the strain energy of the shell can be expressed by

$$U^e = \frac{E}{2(1-\nu^2)} \int_0^l \int_0^{2\pi} [(\epsilon_{ss}{}^e + \epsilon_{\theta\theta}{}^e)^2 - 2(1-\nu)\epsilon_{ss}{}^e\epsilon_{\theta\theta}{}^e]hrd\theta ds + \frac{E}{24(1-\nu^2)} \times \int_0^l \int_0^{2\pi} [(\kappa_{ss}{}^e + \kappa_{\theta\theta}{}^e)^2 - 2(1-\nu)\kappa_{ss}{}^e\kappa_{\theta\theta}{}^e]h^3 rd\theta ds \tag{5}$$

and the work done by the uniform pressure loading, p, in deforming the shell is

$$W^e = \int_0^l \int_0^{2\pi} pw^e rd\theta ds \tag{6}$$

By using the initial load state displacement functions given in Eqs. (2) in conjunction with the strain-displacement relations given in Eqs. (3), the expressions for the strain energy and external work can be written in matrix form as

$$U^e = \tfrac{1}{2}\{a^e\}^T[\bar{K}^e]\{a^e\};\ W^e = \{a^e\}^T\{\bar{Q}\} \tag{7}$$

These equations may be altered to a more familiar form by using the equations which relate the coefficients in the assumed displacement functions, Eqs. (2), to the initial load state nodal displacements for any given element

$$\{q^e\} = [\psi_e]^{-1}\{a^e\} \tag{8}$$

where

$$[\psi_e]^{-1} = \begin{bmatrix} 0 & 0 & 0 & 0 & 1 & 0 \\ 1 & 0 & 0 & 0 & 0 & 0 \\ 0 & 1 & 0 & 0 & -d\varphi^i/ds & 0 \\ 0 & 0 & 0 & 0 & 1 & l \\ 1 & l & l^2 & l^3 & 0 & 0 \\ 0 & 1 & 2l & 3l^2 & -d\varphi^{i+1}/ds & -ld\varphi^{i+1}/ds \end{bmatrix} \tag{9}$$

The altered form of the energy and work expressions is

$$U^e = \tfrac{1}{2}\{q^e\}^T[\psi_e]^T[\bar{K}^e][\psi_e]\{q^e\} = \tfrac{1}{2}\{q^e\}^T[K^e]\{q^e\} \tag{10}$$

$$W^e = \{q^e\}^T[\psi_e]^T\{\bar{Q}\} = \{q^e\}^T\{Q\}$$

Using the minimum potential energy theorem

$$\delta(U^e - W^e) = \{\partial U^e/\partial q^e - \partial W^e/\partial q^e\}\{\delta q^e\}^T = 0 \tag{11}$$

gives the equilibrium equations for the initial load state

$$[K^e]\{q^e\} - \{Q\} = 0 \tag{12}$$

The nodal displacements caused by the initial loading are given by

$$\{q^e\} = [K^e]^{-1}\{Q\} \tag{13}$$

The stress resultants developed in the shell are computed by first calculating the initial load state strains from these displacements and the strain-displacement relations, Eqs. (3), and then by using the constitutive relations

$$\begin{aligned} N_{\theta\theta}{}^e &= [Eh/(1-\nu^2)](\epsilon_{\theta\theta}{}^e + \nu\epsilon_{ss}{}^e) \\ N_{ss}{}^e &= [Eh/(1-\nu^2)](\epsilon_{ss}{}^e + \nu\epsilon_{\theta\theta}{}^e) \\ M_{\theta\theta}{}^e &= [Eh^3/12(1-\nu^2)](\kappa_{\theta\theta}{}^e + \nu\kappa_{ss}{}^e) \\ M_{ss}{}^e &= [Eh^3/12(1-\nu^2)](\kappa_{ss}{}^e + \nu\kappa_{\theta\theta}{}^e) \end{aligned} \tag{14}$$

Combining Eqs. (3) and (14) also gives the convenient relation

$$\beta_s{}^e = 12r(\nu M_{ss}{}^e - M_{\theta\theta}{}^e)/Eh^3 \cos\varphi \tag{15}$$

Perturbed Displacement State

The vibration (or buckling) problem is formulated by perturbing the initial load state displacements, giving the total displacement field

$$u^p = u^e + u;\ v^p = v;\ w^p = w^e + w;\ \beta_s{}^p = \beta_s{}^e + \beta_s \tag{16}$$

or

$$\{q^p\} = \{q^e\} + \{q\} \tag{17}$$

For the perturbed state, the nonlinear form of Sanders' shell equations are used to allow for large rotations of the shell surface. Accordingly, the strain-displacement relations used in the perturbed state are

$$\epsilon_{\theta\theta} = (1/r)[u^p \cos\varphi + (\partial v^p/\partial\theta) + w^p \sin\varphi] + \tfrac{1}{2}(\beta_\theta{}^p)^2 + (1/8r^2)[\partial u^p/\partial\theta - v^p \cos\varphi - r\partial v^p/\partial s]^2 \tag{18a}$$

$$\epsilon_{ss} = [\partial u^p/\partial s + w^p(d\varphi/ds) + \tfrac{1}{2}(\beta_s{}^p)^2 + (1/8r^2)[(\partial u^p/\partial\theta) - v^p \cos\varphi - r\partial v^p/\partial s]^2 \tag{18b}$$

$$\epsilon_{\theta s} = \tfrac{1}{2}\beta_\theta{}^p\beta_s{}^p + (1/2r)[\partial u^p/\partial\theta - v^p \cos\varphi + r\partial v^p/\partial s] \tag{18c}$$

$$\kappa_{\theta\theta} = -(1/r)[\beta_s{}^p \cos\varphi + \partial\beta_\theta{}^p/\partial\theta],\ \kappa_{ss} = -\partial\beta_s{}^p/\partial s \tag{18d}$$

$$\kappa_{\theta s} = -(1/2r)[\partial\beta_s{}^p/\partial\theta - \beta_\theta{}^p \cos\varphi + r\partial\beta_\theta{}^p/\partial s] + (1/4r^2)[rd\varphi/ds - \sin\varphi][\partial u^p/\partial\theta - v^p \cos\varphi - r\partial v^p/\partial s] \tag{18e}$$

where the total rotations are given by

$$\begin{aligned} \beta_s{}^p &= \partial w^p/\partial s - u^p d\varphi/ds \\ \beta_\theta{}^p &= (1/r)(\partial w^p/\partial\theta - v^p \sin\varphi) \end{aligned} \tag{19}$$

If the total displacements given by Eqs. (16) are substituted into these nonlinear equations, the strains and curvatures can be written in the following form, with the initial loading terms again being linearized,

$$\epsilon_{\theta\theta} = \epsilon_{\theta\theta}{}^e + \epsilon_{\theta\theta}{}^{(1)} + \epsilon_{\theta\theta}{}^{(2)} \tag{20a}$$

$$\epsilon_{ss} = \epsilon_{ss}{}^e + \epsilon_{ss}{}^{(1)} + \epsilon_{ss}{}^{(2)} + \beta_s{}^e\beta_s \tag{20b}$$

$$\epsilon_{\theta s} = \epsilon_{\theta s}{}^{(1)} + \epsilon_{\theta s}{}^{(2)} + \tfrac{1}{2}\beta_s{}^e\beta_\theta;\ \kappa_{\theta\theta} = \kappa_{\theta\theta}{}^e + \kappa_{\theta\theta}{}^{(1)} \tag{20c}$$

$$\kappa_{ss} = \kappa_{ss}{}^e + \kappa_{ss}{}^{(1)};\ \kappa_{\theta s} = \kappa_{\theta s}{}^{(1)} \tag{20d}$$

where

$$\begin{aligned} \epsilon_{\theta\theta}{}^{(1)} &= (1/r)[u \cos\varphi + \partial v/\partial\theta + w \sin\varphi] \\ \epsilon_{\theta\theta}{}^{(2)} &= \tfrac{1}{2}\beta_\theta{}^2 + (1/8r^2)[\partial u/\partial\theta - v \cos\varphi - r\partial v/\partial s]^2 \\ \epsilon_{ss}{}^{(1)} &= [\partial u/\partial s + wd\varphi/ds] \\ \epsilon_{ss}{}^{(2)} &= \tfrac{1}{2}\beta_s{}^2 + (1/8r^2)[\partial u/\partial\theta - v \cos\varphi - r\partial v/\partial s]^2 \\ \epsilon_{\theta s}{}^{(1)} &= (1/2r)[\partial u/\partial\theta - v \cos\varphi + r\partial v/\partial s] \\ \epsilon_{\theta s}{}^{(2)} &= \tfrac{1}{2}\beta_\theta\beta_s \end{aligned} \tag{21a}$$

$$\kappa_{\theta\theta}{}^{(1)} = -(1/r)[\beta_s \cos\varphi + \partial\beta_\theta/\partial\theta];\ \kappa_{ss}{}^{(1)} = -\partial\beta_s/\partial s \tag{21b}$$

$$\kappa_{\theta s}{}^{(1)} = -(1/2r)[\partial\beta_s/\partial\theta - \beta_\theta \cos\varphi + r\partial\beta_\theta/\partial s] + (1/4r^2)[r(d\varphi/ds) - \sin\varphi][\partial u/\partial\theta - v \cos\varphi - r\partial v/\partial s] \tag{21c}$$

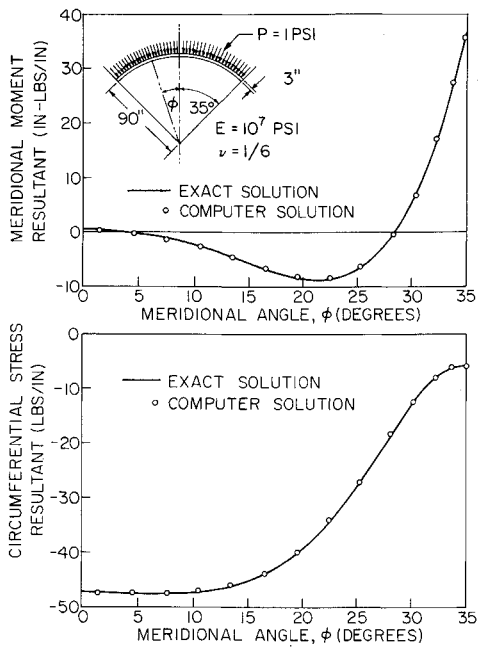

Fig. 2 Comparison of computer and theoretical solutions to the problem of stresses in a clamped, externally pressurized spherical cap.

The superscripts (1) and (2) refer to the terms which are linear and quadratic functions of the perturbation displacements, respectively, while terms with the superscript e are those which are independent of the perturbations and are identical to their counterparts in the initial load state. The perturbation rotations in the meridional and circumferential directions, respectively, are given by

$$\beta_s = \beta_s{}^p - \beta_s{}^e = [\partial w/\partial s - u(d\varphi/ds)]$$
$$\beta_\theta = \beta_\theta{}^p = (1/r)[\partial w/\partial\theta - v\sin\varphi] \tag{22}$$

With the existence of the asymmetric displacements in the nth harmonic, the strain energy becomes

$$U = \frac{E}{2(1-\nu^2)}\int_0^l\int_0^{2\pi}\{(\epsilon_{\theta\theta}+\epsilon_{ss})^2 - 2(1-\nu)\times [\epsilon_{\theta\theta}\epsilon_{ss} - (\epsilon_{\theta s})^2]\}hrd\theta ds + \frac{E}{24(1-\nu^2)}\times \int_0^l\int_0^{2\pi}\{(\kappa_{\theta\theta}+\kappa_{ss})^2 - 2(1-\nu)[\kappa_{\theta\theta}\kappa_{ss} - (\kappa_{\theta s})^2]\}h^3rd\theta ds \tag{23}$$

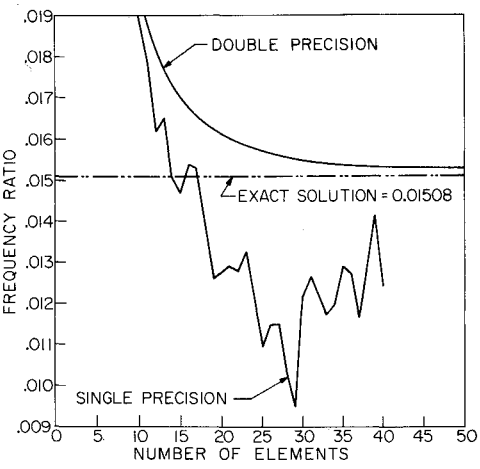

Fig. 3 Finite element convergence of the first mode lowest natural frequency of a clamped cylinder with physical proportions $L/R = 10$ and $R/T = 500$.

and the work done by the uniform pressure loads in further deforming the shell to the final perturbed position is given by[7]

$$W = p\int_0^l\int_0^{2\pi}\left\{w^p r - \frac{1}{2}[u^p\beta_s{}^p + v^p\beta_\theta{}^p - w^p(\epsilon_{\theta\theta}+\epsilon_{ss})]\right\}rd\theta ds \tag{24}$$

Substitution of Eqs. (14, 15, 20, and 22) into Eqs. (23) and (24) gives the result

$$U = U^e + U^{(2)} + U_\sigma{}^{(2)} + \text{higher order terms}$$
$$W = W^e + W^{(2)} + \text{higher order terms} \tag{25}$$

where

$$U^{(2)} = \frac{E}{2(1-\nu^2)}\int_0^l\int_0^{2\pi}[[\epsilon_{\theta\theta}{}^{(1)} + \epsilon_{ss}{}^{(1)}]^2 - 2(1-\nu)\{\epsilon_{\theta\theta}{}^{(1)}\epsilon_{ss}{}^{(1)} - [\epsilon_{\theta s}{}^{(1)}]^2\}]hrd\theta ds + \frac{E}{24(1-\nu^2)}\int_0^l\int_0^{2\pi}[[\kappa_{\theta\theta}{}^{(1)} + \kappa_{ss}{}^{(1)}]^2 - 2(1-\nu)\{\kappa_{\theta\theta}{}^{(1)}\kappa_{ss}{}^{(1)} - [\kappa_{\theta s}{}^{(1)}]^2\}]h^3rd\theta ds \tag{26}$$

$$U_\sigma{}^{(2)} = N_{ss}{}^e\int_0^l\int_0^{2\pi}\epsilon_{ss}{}^{(2)}rd\theta ds + N_{\theta\theta}{}^e\int_0^l\int_0^{2\pi}\epsilon_{\theta\theta}{}^{(2)}rd\theta ds - \frac{12(M_{\theta\theta}{}^e - \nu M_{ss}{}^e)}{(1-\nu^2)}\int_0^l\int_0^{2\pi}\{[\epsilon_{ss}{}^{(1)} + \nu\epsilon_{\theta\theta}{}^{(1)}]\beta_s + (1-\nu)\beta_\theta\epsilon_{\theta s}{}^{(1)}\}\frac{r^2d\theta ds}{h^2\cos\varphi} \tag{27}$$

$$W^{(2)} = -\frac{p}{2}\int_0^l\int_0^{2\pi}\{u\beta_s + v\beta_\theta - w[\epsilon_{\theta\theta}{}^{(1)} + \epsilon_{ss}{}^{(1)}]\}rd\theta ds \tag{28}$$

Since the perturbation displacements are harmonic functions, the kinetic energy for the conservative system is given by

$$T = \frac{\rho}{2}\int_0^l\int_0^{2\pi}(v_s{}^2 + v_\theta{}^2 + v_z{}^2)hrd\theta ds \tag{29}$$

where the velocity components are

$$v_s = \partial u/\partial t = i\omega u;\ v_\theta = \partial v/\partial t = i\omega v;\ v_z = \partial w/\partial t = i\omega w \tag{30}$$

The substitution of Eqs. (1) and (21) into Eqs. (26–29) reveals that these latter expressions are each quadratic in the perturbation displacements. Manipulating the equations which so result, it is possible to write Eqs. (25) and (29) in matrix form. With the higher order terms being omitted, Eqs. (25) and (29) become

$$U = U^e + \tfrac{1}{2}\{a\}^T[\bar{K}]\{a\} + \tfrac{1}{2}\{a\}^T[\bar{K}_\sigma]\{a\} \tag{31a}$$
$$W = W^e + \tfrac{1}{2}\{a\}^T[\bar{N}]\{a\};\ T = -(\omega^2/2)\{a\}^T[\bar{M}]\{a\} \tag{31b}$$

As in the case of the initial load state, these equations may also be altered to a more familiar form by using the equations which relate the coefficients in the assumed displacement functions, Eqs. (1), to the perturbation nodal displacements for any given element

$$\{q\} = [\psi]^{-1}\{a\} \tag{32}$$

where

$$[\psi]^{-1} = \begin{bmatrix} 0 & 0 & 0 & 0 & 1 & 0 & 0 & 0 \\ 0 & 0 & 0 & 0 & 0 & 0 & 1 & 0 \\ 1 & 0 & 0 & 0 & 0 & 0 & 0 & 0 \\ 0 & 1 & 0 & 0 & -d\varphi^i/ds & 0 & 0 & 0 \\ 0 & 0 & 0 & 0 & 1 & l & 0 & 0 \\ 0 & 0 & 0 & 0 & 0 & 0 & 1 & l \\ 1 & l & l^2 & l^3 & 0 & 0 & 0 & 0 \\ 0 & 1 & 2l & 3l^2 & -d\varphi^{i+1}/ds & -ld\varphi^{i+1}/ds & 0 & 0 \end{bmatrix} \tag{33}$$

The altered form of the energy and work expressions is

$$U = U^e + \tfrac{1}{2}\{q\}^T[\psi]^T[\bar{K}][\psi]\{q\} + \tfrac{1}{2}\{q\}^T[\psi]^T[\bar{K}_\sigma][\psi]\{q\}$$
$$= U^e + \tfrac{1}{2}\{q\}^T[K]\{q\} + \tfrac{1}{2}\{q\}^T[K_\sigma]\{q\} \quad (34)$$

$$W = W^e + \tfrac{1}{2}\{q\}^T[\psi]^T[\bar{N}][\psi]\{q\}$$
$$= W^e + \tfrac{1}{2}\{q\}^T[N]\{q\} \quad (35)$$

$$T = -(\omega^2/2)\{q\}^T[\psi]^T[\bar{M}][\psi]\{q\}$$
$$= -(\omega^2/2)\{q\}^T[M]\{q\} \quad (36)$$

Using Lagrange's equation for the conservative system

$$(d/dt)\{\partial T/\partial \dot{q}\} - \{\partial T/\partial q\} + \{\partial U/\partial q\} = \{\partial W/\partial q\} \quad (37)$$

gives the equilibrium equations for the perturbed displacement state

$$-\omega^2[M]\{q\} + [K]\{q\} + [K_\sigma]\{q\} = [N]\{q\} \quad (38)$$

This equation is seen to differ from that of the usual free vibrations problem in the addition of the two matrices, the geometric stiffness matrix, $[K_\sigma]$, and the uniform pressure work matrix, $[N]$, each term of which is linearly dependent on the initial pressure loading. Because the initial load state has been linearized, these two load dependent matrices can be expressed in the load independent form

$$[L'] = [K_\sigma] - [N] = p[K_\sigma'] - p[N'] = p[L] \quad (39)$$

and Eq. (38) is written as

$$[-\omega^2 M + K + pL]\{q\} = 0 \quad (40)$$

The eigenvalue problem for the free vibrations of the initially pressurized shell is, therefore, given by

$$|-\omega^2[I] + [M]^{-1}[K + pL]| = 0 \quad (41)$$

The critical buckling pressure is obtained for the limiting case of zero natural frequency, i.e., $\omega = 0$, and is expressed as the eigenvalue problem

$$|-p[I] + [L]^{-1}[K]| = 0 \quad (42)$$

Computer Program

A large capacity finite element computer program was written[8] to perform the computations required to solve the initial loading problem, defined by Eq. (13), and the vibration and buckling problems, defined by Eqs. (41) and (42), respectively. Since the paraboloid meridional geometry varies continuously along the length of the shell, the integrals for the energy and work expressions given in Eqs. (26–29) cannot be evaluated exactly. The stiffness, work and inertia matrices' coefficients, which are derived from the foregoing expressions, are therefore expressed in integral form and must be numerically evaluated by the computer. For all such integrations, the Newton-Cotes seven point integration formula is used. The Cholesky square root method is used to solve the initial load state, since it directly determines the nodal displacement vector in Eq. (13) without explicitly inverting the large, narrowly banded initial load state stiffness matrix. For the vibrations problem, a symmetric dynamical matrix is formed by decomposing the inertia matrix into an upper and lower triangular form, rather than inverting it as is shown for convenience in Eq. (41). The same decomposition is used in Eq. (42) to produce a symmetric buckling matrix. The Givens method is used to solve these two eigenvalue problems, because it is very rapid and also makes use of the symmetry of the dynamical and buckling matrices, thereby considerably reducing both the execution time and the required computer core storage. With the IBM 360 model 65 digital computer being used for the calculations, double precision arithmetic is needed to preserve computational accuracy when the number of finite elements, required for convergence, are used (see Fig. 3).

Table 1 Paraboloidal shell test specimens

Test shell number	Focal length, in.	Open end diameter, in.	Nominal thickness, in.
1	1.7234	15.88	0.028
2	1.7234	16.06	0.064
3	1.7234	13.06	0.047

To demonstrate the accuracy and versatility of the computer program, several example problems are chosen from the available literature to be analyzed and compared to the given solutions. Of these, the ones of most interest are those that relate most closely to the problem at hand, i.e., the free vibrations of the clamped, pressure loaded shell. Accordingly three such sample problems are included in this discussion. The first of these is taken from Timoshenko[9] and is the calculation of the stresses in a clamped spherical cap, loaded externally by a uniform pressure. For the analysis, 35 finite elements are used, with both the computer and the theoretical results for the meridional moment resultant and the circumferential stress resultant being shown in Fig. 2.

The second problem chosen for comparison purposes is taken from Sobel[10] and is the calculation of the critical buckling load for a clamped cylinder, loaded externally by a uniform pressure. The critical pressure given in the reference, for a clamped cylinder having a length to radius ratio of four, is $P_{cr} = (0.0003351)\ Eh/R$ occurring at the fifth harmonic. The solution predicted by the computer program using 18 finite elements also occurs at $n = 5$ and is $P_{cr} = (0.0003359)\ Eh/R$, which is less than one-quarter of 1% different from that given by Sobel.

The final case chosen for comparison purposes is the free vibrations of a clamped cylindrical shell. For such a cylinder, having a length to radius ratio of ten and a radius to thickness ratio of 500, Forsberg[11] gives an exact solution, for the frequency ratio $\omega R[\rho(1 - \nu^2)/E]^{1/2}$, of 0.01508, with a corresponding mode shape, normalized on the normal displacement, of u max $= \pm 0.01799$ and v max $= -0.2507$. Using 35 elements, the computed solution, for a clamped cylinder with the same proportions, is 0.01537 with a corresponding mode shape of u max $= \pm 0.01807$ and v max $= -0.2510$ when normalized on the normal displacement w. The results are, therefore, less than 2% in error for the frequency and less than one-half of 1% in error for the mode shape. The convergence of this finite element solution, as well as the loss of numerical accuracy when single precision arithmetic is used, is shown in Fig. 3.

Experimental Investigation

An extensive experimental program was conducted to accumulate data for use in ascertaining the validity of the computer results. Three different paraboloidal shells were used in the tests, each having the equation $r^2 = 6.8936\chi$ for its generator. Each of the test shells was an 1100-O aluminum spinning, and the respective radii and thickness are given in Table 1. During the experiments, the shells were clamped to a plate and an external pressure was applied by evacuating the interior of the shells using a vacuum pump. The clamping and sealing of the shells was accomplished by filling the circular mounting groove, into which the free edge of the paraboloid had been fit, with a low-melting point, bismuth alloy.

The shells were excited by an electromagnet, with the frequencies being monitored with an electronic counter and the pressures with a mercury manometer. The response of the shells was measured with a microphone, positioned in the immediate proximity to the vibrating specimen. By centering the mounted paraboloids beneath a spider-like fixture which supported the microphone on a rotary arm, the com-

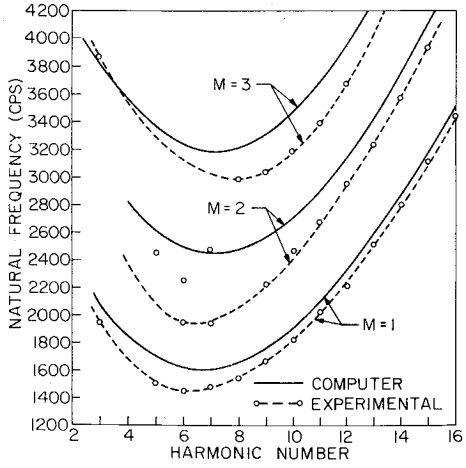

Fig. 4 Comparison of finite element and experimental results for the lowest three mode natural frequencies of paraboloidal test shell number two with a pressure of 4.8 psi applied.

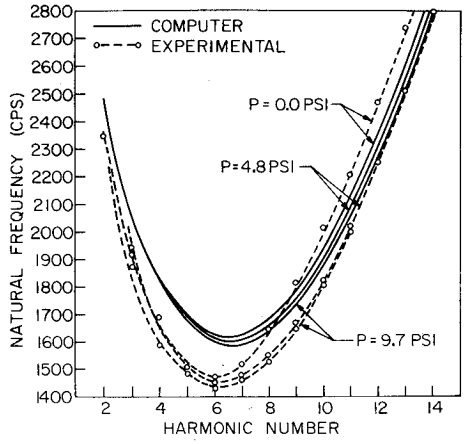

Fig. 6 Comparison of finite element and experimental results for the lowest mode natural frequencies of paraboloidal test shell number two with different pressures applied.

plete circumferential mode shape at a single point along the meridian was measured and recorded at each frequency for which a resonant rise was detected. These rises in the response spectrums, detected by monitoring the microphone output on an oscilloscope, were determined for the lowest three vibration modes of each of the test shells.

Results

The essential findings of the analytical and experimental studies are presented in Figs. 4–8. For the most part, only the results for the first mode have been given, since those for the higher modes are generally not in good agreement. The curves shown in Fig. 4, which represent the first three modes for test shell number two with a uniform external pressure of 4.8 psi applied over the surface, are an exception to this general trend. In addition to exhibiting this unusually good agreement between the two results, these curves also show several noteworthy trends which are common to all the results obtained. The most significant of these is that the shape of all of the frequency-harmonic curves obtained exhibit the characteristics predicted by Gol'denveizer[12] for shells having a positive meridional Gaussian curvature. The shape of these curves, as predicted by this reference and verified in the current study, is an initially decreasing natural frequency with an increasing harmonic number until some minimum value is reached, from which point the frequency increases monotonically as the harmonic number is further increased.

Figure 4 also shows that the computer results, for which 35 finite elements are used in all the paraboloid calculations, are for the most part higher than those obtained from the experiments. One of the reasons for this behavior is that the finite element solutions, which are obtained from an energy derivation, converge to the correct solution from values greater than the true value, as is shown in Fig. 3. However, the computed solutions for the paraboloid geometries included in the present investigation are all found to be very close to convergence for the 35 finite elements used, i.e., the solution curves for the paraboloids exhibit the same rate of convergence as does the cylinder solution shown in Fig. 3. Therefore, the difference between the experimental and computer solutions is primarily attributed to the fact that the latter results are based on a totally clamped boundary condition at the outer edge which was probably not achieved experimentally. Evidence of deterioration of the fully clamped boundary condition was found in both the vibration tests[8] and in a series of buckling experiments[13] subsequently performed on truncated paraboloidal shells of the same focal length and mounted in the same manner as those used in this study. In the vibration tests, the measured natural frequencies were often found to decrease after the shell had been subjected to successive external pressure loading cycles. A sample of such a decrease can be seen by comparing the three minimum natural frequencies on the three respective pressure curves in Fig. 5 with the three frequencies measured at the same pressures applied to the same shell several loading cycles later and shown in Fig. 8. In the aforementioned buckling experiments,[13] there was

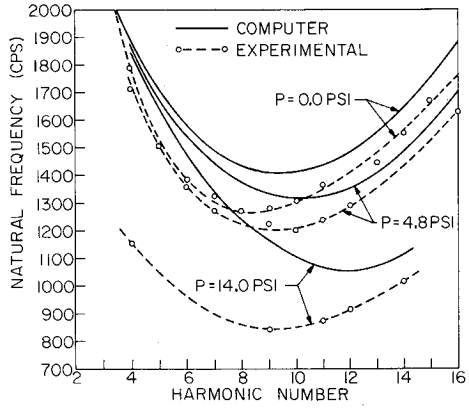

Fig. 5 Comparison of finite element and experimental results for the lowest mode natural frequencies of paraboloidal test shell number one with different pressures applied.

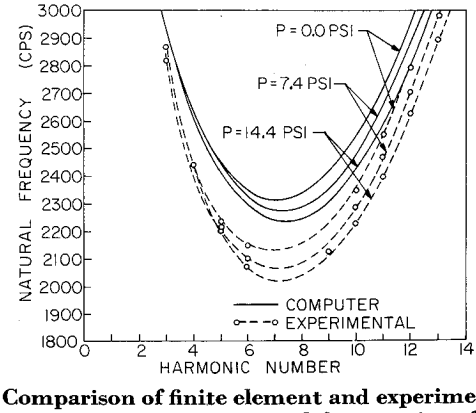

Fig. 7 Comparison of finite element and experimental results for the lowest mode natural frequencies of paraboloidal test shell number three with different pressures applied.

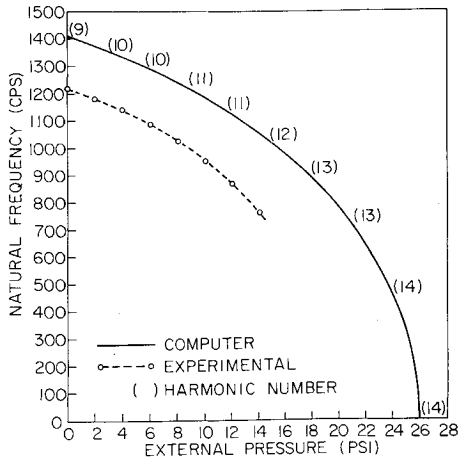

Fig. 8 Comparison of finite element and experimental results for the first mode pressure vs natural frequency data for paraboloidal test shell number one.

observable slippage of the in-plane shell displacements at the boundary attachment to the bismuth alloy.

Figures 5–7 give the first mode comparisons between the computed and experimental results for the three test shells. The minimum natural frequencies measured in the experiments are in every case about 10% lower than their theoretical counterparts calculated with the same applied pressure loadings. Good agreement is also gotten for the harmonic number at which the corresponding minimum frequencies occur, and in all cases, the natural frequencies are seen to be reduced by increasing the externally applied pressure loading. For all three shells, the drop in frequency is approximately proportional to the corresponding increase in the external pressure in the load ranges considered, i.e., the natural frequency-external pressure curves, such as that shown in Fig. 8, are approximately linear in the low-load region. Because the method chosen for pressurizing the test shells consisted of evacuating the enclosed volumes and accordingly limited the external loading to about 14.5 psi, it was not possible to extend the test results to the buckling region. However, this exercise was performed analytically, with the results being shown in Fig. 8. Again allowing for a reasonable difference between the analytical and experimental results, good agreement is found between the two results. As was shown in previous research with other shell geometries,[1–15] the pressure-frequency curve, which is approximately linear in the low-pressure region, becomes highly nonlinear as the pressure approaches the critical buckling value, i.e., the natural frequency approaches zero.

Conclusions

In view of the excellent results obtained for the finite element stress, buckling and vibrations analyses of shell problems with known, published solutions, it is clear that the finite element method can be used to accurately predict the first mode natural frequencies of a paraboloidal shell subjected to an external pressure loading (providing sufficient care is exercised not to lose computational accuracy for large problems). Accounting for apparently explainable differences between analytical and experimental results, this accuracy has further been demonstrated in the laboratory. Regardless of the magnitude of the pressure loading, the shape of the natural frequency-harmonic curve continues to conform to that which is theoretically predicted for all shells having a positive meridional Gaussian curvature. Increasing the external pressure loading is found to lower the natural frequencies of the shell, in a nearly linear relation at low pressures, but in a highly nonlinear fashion as the pressure approaches the critical buckling value.

It is not entirely clear why the agreement between the computed and experimental results for modes greater than the first is so much poorer than that obtained for the first or lowest mode. While it is possible that one of the reasons for this is poorer convergence of the analytical solutions for the higher modes, further investigation of the effects of the boundary conditions (particularly on these higher modes) is in order. In any case, it is apparent that the externally applied pressure loading does materially effect the vibration characteristics of the paraboloidal shells, and should accordingly be accounted for in any such dynamic analysis.

References

[1] Armenákas, A. E., "Influence of Initial Stress on the Vibrations of Simply Supported Circular Cylindrical Shells," *AIAA Journal*, Vol. 2, No. 9, Sept. 1964, pp. 1607–1612.

[2] Armenákas, A. E. and Herrmann, G., "Vibrations of Infinitely Long Cylindrical Shells Under Initial Stress," *AIAA Journal*, Vol. 1, No. 1, Jan. 1963, pp. 100–106.

[3] Archer, R. R., "On the Influence of Uniform Stress States on the Natural Frequencies of Spherical Shells," *Journal of Applied Mechanics*, Vol. 29, No. 3, Sept. 1962, pp. 502–505.

[4] Archer, R. R. and Famili, J., "On the Vibration and Stability of Finitely Deformed Shallow Spherical Shells," *Journal of Applied Mechanics*, Vol. 32, No. 1, March 1965, pp. 116–120.

[5] Okubo, S. and Whittier, J. S., "A Note on Buckling and Vibrations of an Externally Pressurized Shallow Spherical Shell," *Journal of Applied Mechanics*, Vol. 34, No. 4, Dec. 1967, pp. 1032–1034.

[6] Sanders, J. L., Jr., "Nonlinear Theories for Thin Shells," *Quarterly of Applied Mathematics*, Vol. 21, No. 1, 1963, pp. 21–36.

[7] Navaratna, D. R., "Elastic Stability of Shells of Revolution by the Variational Approach Using Discrete Elements," BSD-TR-66-261, June 1966, MIT.

[8] Margolias, D. S., "The Effect of External Loading on the Natural Frequencies of Paraboloidal Shells," Ph.D. thesis, 1970, Univ. of Southern California, Los Angeles Calif.

[9] Timoshenko, S. P. and Woinowsky-Krieger, S., *Theory of Plates and Shells*, McGraw-Hill, New York, 1959, pp. 553–554.

[10] Sobel, L. H., "Effects of Boundary Conditions on the Stability of Cylinders Subject to Lateral and Axial Pressures," TR 6-90-63-91, Sept. 1963, Lockheed Missiles & Space Co., Palo Alto, Calif.

[11] Forsberg, K., "A Review of Analytical Methods Used to Determine the Model Characteristics of Cylindrical Shells," TR 6-75-65-25, May 1965, Lockheed Missiles & Space Co., Palo Alto, Calif.

[12] Gol'denveizer, A. L., "Asymptotic Properties of Eigenvalues in Problems of the Theory of Thin Elastic Shells," *Applied Mathematics and Mechanics*, Vol. 25, No. 4, 1961, pp. 1077–1094.

[13] Stocco, F., "Experimental Determination of the Buckling of Thin-Walled Truncated Paraboloidal Shells Under Combined External Pressure and Axial Compression," Masters' thesis, Jan. 1970, Dept. of Aerospace Engineering, Univ. of Southern California, Los Angeles, Calif.